GMR
The Original

ANTIDIABETIC POTENTIAL OF SUSTAINABLE STARCH/PVA/CuO ELECTROSPUN NANOSCAFFOLDS FROM *Sargassum wightii* EXTRACT

Hanisha Govindaraj[1], Sanjay Surya R[2], Alagendran Subbarayalu[3]*

[1]Saveetha Medical College & Hospital (SMCH), Saveetha Institute of Medical and Technical Sciences (SIMATS), Thandalam, Chennai, Tamil Nadu 602105, India. sandheepselvarks06@gmail.com
[2]Department of Anaesthesiology, Saveetha Medical College and Hospital, Saveetha Institute of Medical And Technical Sciences (SIMATS), Thandalam, Chennai-602105, Tamil Nadu, India. Email: sanjaysurya1997@gmail.com; ORCID: https://orcid.org/0009-0005-9187-8496.
[3]Clinical Neuroscience and Phytomedicine Laboratory, Department of Research, Saveetha College of Nursing (SCON), Saveetha Institute of Medical and Technical Sciences (SIMATS), Chennai 602105, Tamil Nadu, India. Email: proteinblg@gmail.com; alagendrans.scon@saveetha.com. ORCID: https://orcid.org/0009-0009-0749-7180.
*Correspondence: proteinblg@gmail.com; alagendrans.scon@saveetha.com (A.S.)

ABSTRACT
This study investigated the green synthesis of copper oxide nanoparticles (CuO NPs) using *Sargassum wightii* algal extract and their incorporation into starch/PVA nanoscaffolds for antidiabetic applications. UV-Visible spectroscopy confirmed CuO NP formation with a characteristic surface plasmon resonance peak at 292 nm, while Fourier-transform infrared spectroscopy (FTIR) analysis revealed functional groups involved in stabilization and scaffold integration. X-ray diffraction (XRD) confirmed the monoclinic tenorite phase of CuO NPs, with nanoscaffolds exhibiting semi-crystalline structure (45.3% crystallinity). scanning electron microscopy (SEM) imaging showed uniform, spherical CuO NPs and porous nanofibrous scaffolds (150–200 nm fiber diameter), ensuring optimal nanoparticle dispersion. Thermogravimetric analysis (TGA) indicated scaffold stability up to 220°C, while DLS and zeta potential measurements demonstrated excellent colloidal stability (−12.0 mV). Antidiabetic evaluation revealed concentration-dependent α-amylase inhibition, with nanoscaffolds exhibiting the highest activity (78.52% at 100 µg/mL), surpassing CuO NPs (68.52%) and algal extract (50.52%). Similar trends were observed in α-glucosidase inhibition assays. The enhanced efficacy of nanoscaffolds is attributed to synergistic interactions between CuO NPs and the polymer matrix. These findings highlight the potential of starch/PVA/CuO-NPs nanoscaffolds as effective antidiabetic agents, warranting further in vivo studies for therapeutic validation.

KEYWORDS: *Sargassum wightii*, Green synthesis, CuO NPs, Starch/PVA/CuO-NPs nanoscaffolds, Antidiabetic activity.

1. INTRODUCTION

Diabetes mellitus is a chronic metabolic disorder characterized by impaired insulin secretion or action, resulting in elevated blood glucose levels and associated complications such as cardiovascular diseases, neuropathy, and nephropathy [1]. The global prevalence of diabetes continues to rise at an alarming rate, posing significant health, economic, and social burdens worldwide [2]. According to the International Diabetes Federation, over 500 million adults were living with diabetes as of 2021, and this number is expected to escalate further in the coming decades [3]. Despite numerous advancements in pharmaceutical therapies, managing diabetes remains challenging due to side effects, drug resistance, and limited accessibility in resource-constrained regions [4]. Consequently, there is an urgent demand for innovative, cost-effective, and biocompatible antidiabetic strategies that can effectively regulate blood glucose levels while minimizing adverse effects [5].

In recent years, nanotechnology has emerged as a promising platform for addressing complex biomedical challenges, including diabetes management [6]. Nanomaterials, due to their unique physicochemical properties such as high surface area-to-volume ratio, tunable surface functionalities, and enhanced bioavailability, offer new avenues for designing advanced therapeutic agents [7]. Among various nanomaterials, copper oxide nanoparticles (CuO NPs) have attracted considerable attention owing to their potent biological activities, including antimicrobial, antioxidant, and enzyme inhibitory effects [8]. These properties suggest CuO NPs as promising candidates for modulating key enzymes involved in carbohydrate metabolism, such as α-amylase and α-glucosidase [9], which

play pivotal roles in postprandial glucose regulation by catalyzing starch and disaccharide breakdown into absorbable glucose units [10].

The synthesis of CuO NPs using conventional physical and chemical methods, however, often involves hazardous reagents, elevated energy consumption, and generates toxic by-products, which limit their biomedical applications [11]. In this context, green synthesis approaches utilizing biological resources such as plants, algae, and microorganisms have gained momentum as sustainable and eco-friendly alternatives [12]. Marine macroalgae, in particular, are rich sources of diverse bioactive compounds, including polysaccharides, polyphenols, vitamins, and minerals, which can act as natural reducing and stabilizing agents in nanoparticle synthesis [13]. *Sargassum wightii*, a brown macroalga abundant along the Indian coastal regions, is recognized for its pharmacological properties such as antioxidant, anti-inflammatory, and antidiabetic effects [14]. Leveraging the biomolecules present in *S. wightii* extract to mediate the synthesis of CuO NPs can not only minimize environmental impact but also impart additional bioactivity to the nanoparticles through surface functionalization, enhancing their therapeutic potential [15].

Electrospinning is a versatile and straightforward technique to fabricate nanofibrous scaffolds with high porosity, interconnected pore structures, and large surface area, which closely mimic the native extracellular matrix (ECM) [16]. These scaffolds can serve as effective delivery platforms for bioactive nanoparticles, providing sustained release and enhanced interaction with biological targets [17]. Polyvinyl alcohol (PVA), a synthetic, water-soluble, and biocompatible polymer, is widely employed in electrospinning due to its excellent film-forming ability, mechanical strength, and non-toxicity [18]. The incorporation of natural polymers like starch, a biodegradable polysaccharide, into PVA matrices can improve scaffold hydrophilicity, mechanical properties, and biological compatibility, making starch/PVA composites ideal candidates for biomedical applications, including wound healing and drug delivery [19]. Embedding green-synthesized CuO NPs within starch/PVA electrospun nanofibrous scaffolds thus offers a promising approach to develop novel antidiabetic materials that combine the advantages of biocompatible polymers and bioactive nanoparticles [20].

The enzymatic breakdown of dietary carbohydrates by α-amylase and α-glucosidase leads to elevated postprandial blood glucose levels, which are key contributors to hyperglycemia in diabetes [21]. Inhibitors of these enzymes can effectively delay carbohydrate digestion and glucose absorption, thus attenuating hyperglycemic spikes [22]. While synthetic inhibitors like acarbose are clinically used, their side effects including gastrointestinal discomfort and liver toxicity underscore the need for safer alternatives [23]. CuO NPs synthesized via green routes, enriched with bioactive compounds from *S. wightii*, might offer potent inhibitory effects against these enzymes, capitalizing on synergistic interactions between the metal oxide core and algal phytochemicals [24].

Ultrasonic-assisted extraction enhances the yield and activity of bioactive compounds from natural sources by disrupting cellular matrices and facilitating solvent penetration, making it a valuable technique for obtaining efficacious extracts from marine macroalgae [25]. The use of ultrasonic-assisted, *S. wightii*-mediated green synthesis not only improves nanoparticle quality and stability but also ensures eco-friendly production under mild conditions, aligning with the principles of green chemistry [26].

Despite growing interest in the biomedical applications of marine algae-derived nanoparticles, research on integrating green-synthesized CuO NPs into electrospun nanoscaffolds for antidiabetic therapy remains limited [27]. This study aims to address this gap by developing and characterizing starch/PVA electrospun scaffolds embedded with ultrasonic-assisted, *S. wightii*-mediated CuO NPs and evaluating their antidiabetic efficacy through in vitro α-amylase and α-glucosidase inhibition assays. Comprehensive physicochemical characterization including UV-Visible spectroscopy, Fourier-transform infrared spectroscopy (FTIR), X-ray diffraction (XRD), scanning electron microscopy (SEM), thermogravimetric analysis (TGA), and zeta potential measurements will elucidate the structural and functional attributes of the nanoparticles and scaffolds.

By combining the natural bioactivity of *S. wightii* compounds, the therapeutic potential of CuO NPs, and the biocompatibility of starch/PVA nanofibers, this research endeavors to develop an innovative and sustainable nanomaterial-based platform for diabetes management. The findings from this study could pave the way for next-generation antidiabetic therapies that are environmentally friendly, cost-effective, and capable of mitigating diabetes-associated complications through multifunctional mechanisms. Furthermore, this approach exemplifies the integration of marine biotechnology, green nanotechnology, and polymer science in addressing pressing healthcare challenges, highlighting the vast potential of marine resources in drug discovery and delivery.

2. MATERIALS AND METHODS

2.1. Materials

This study utilized *S. wightii* macroalgae collected from the coastal region of Rameswaram, Tamil Nadu, India, serving as the biological agent for green synthesis of CuO NPs. Copper (II) sulfate pentahydrate ($CuSO_4 \cdot 5H_2O$), procured from Sigma-Aldrich, was employed as the copper precursor. PVA with an average molecular weight of

approximately 115,000 was used as the main polymer for electrospinning. Starch, sourced locally, was incorporated to improve scaffold characteristics. Analytical-grade chemicals, including ethanol and Milli-Q water, were acquired from Merck and Sigma-Aldrich. Electrospinning was performed on a HOLMARC HO-NFES-040 system equipped with a syringe pump. Characterization techniques for nanoparticles and scaffolds included UV-Visible spectroscopy (VIS SPEC V-730), FTIR (Spectrum Two, PerkinElmer), XRD (Bruker D8 Advance), SEM (JSM-IT800 NANO), DLS and zeta potential analysis (Malvern Zetasizer Ultra), as well as thermogravimetric analysis (TGA 8000, PerkinElmer). Antidiabetic assays followed established standard protocols.

2.2. Collection of marine macroalgae

Fresh *S. wightii* samples were collected from marine waters near Rameswaram. The biomass was rinsed thoroughly with tap water to remove impurities and epiphytes, followed by multiple washes with distilled water to eliminate any residual debris. Approximately 100 grams of cleaned algae were cut into small pieces and air-dried at ambient temperature for roughly two weeks. The fully dried material was then pulverized into a fine powder using a mechanical grinder and stored in sealed containers for subsequent use.

2.3. Ultrasonic-assisted extraction

For extracting bioactive constituents, 2 grams of powdered *S. wightii* were mixed with 50 mL of Milli-Q water in a 100 mL beaker. The mixture underwent ultrasonic-assisted extraction in a LABQUEST ultrasonic cleaner (Borosil; Serial No. 941032329018) at 60°C for 45 minutes. The extract was filtered through Whatman No. 1 filter paper under sterile conditions, and the clear filtrate was collected and stored at 10°C. To enable long-term storage and future applications, the aqueous extract was freeze-dried using a laboratory lyophilizer [28].

2.4. Green Synthesis of CuO NPs

CuO NPs were synthesized by a green approach utilizing the prepared *S. wightii* extract. In brief, 50 mL of 0.1 M $CuSO_4 \cdot 5H_2O$ solution was combined with 10 mL of *S. wightii* extract (10 mg powder in 10 mL Milli-Q water) at a 5:1 ratio. This mixture was stirred continuously at 650 rpm and maintained at 60°C for 2 hours. The color change from blue to bluish-green visually confirmed nanoparticle formation. The product was washed three times with double-distilled water under the same stirring and temperature conditions to remove unreacted materials. The purified CuO NPs were then freeze-dried for 48 hours and stored as a powder for further characterization and scaffold preparation [29].

2.5. Preparation of CuO-loaded electrospun starch/PVA scaffolds

A 15% (w/w) aqueous solution of PVA was prepared by dissolving the polymer in Milli-Q water under constant stirring. To this solution, 100 mg each of starch and the biosynthesized CuO NPs were added and stirred vigorously at 50°C for 2.5 hours to achieve uniform dispersion. The resulting homogenous mixture was loaded into a syringe fitted with a needle of 0.84 mm inner diameter and electrospun using the HOLMARC HO-NFES-040 system powered by a HMPSKV30 high-voltage power supply (0–30 kV, 0.5 mA). Optimal electrospinning parameters were set to 11.5 kV voltage, 12.3 cm needle-to-collector distance, and a feed rate of 0.4 mL/h. The electrospinning process continued for 6 to 8 hours at room temperature, producing uniform nanofibrous mats [30, 31].

2.6. Physicochemical characterization

2.6.1. UV–Visible spectroscopy

UV–Vis spectroscopy confirmed nanoparticle synthesis and investigated the optical characteristics of both the aqueous *S. wightii* extract and the green-synthesized CuO NPs. Spectra were recorded with a VIS SPEC V-730 spectrophotometer in the 200–800 nm wavelength range, using deionized water as a blank. Surface plasmon resonance (SPR) peaks were analyzed to verify nanoparticle formation and their interaction within the composite scaffold [32].

2.6.2. FTIR spectroscopy analysis

FTIR analysis was performed using a PerkinElmer Spectrum Two instrument in attenuated total reflectance (ATR) mode to identify functional groups and molecular interactions. Spectra of CuO NPs and the CuO-loaded scaffolds were collected between 4000 and 400 cm^{-1} with a resolution of 4 cm^{-1} and 64 scans per sample. Key absorption bands related to hydroxyl, carbonyl, amide, and metal-oxygen bonds were examined [33].

2.6.3. XRD analysis

The crystalline structure and phase purity of synthesized CuO NPs and the scaffolds were characterized using a Bruker D8 Advance XRD system with CuKα radiation ($\lambda = 1.5406$ Å), operating at 40 kV and 40 mA. Diffraction patterns were recorded across a 2θ range of 5° to 90° with a step size of 0.029649°. Peaks corresponding to monoclinic CuO were analyzed alongside any shifts caused by nanoparticle-polymer interactions [34].

2.6.4. SEM analysis

SEM was conducted on a JEOL JSM-IT800 NANO to examine surface morphology, nanoparticle distribution, and fiber alignment within the scaffolds. Samples were sputter-coated with gold to prevent charging before imaging. High-resolution micrographs provided details about particle size, shape, dispersion, and scaffold nanostructure [28].

2.6.5. TGA

Thermal properties of CuO-containing scaffolds were assessed by thermogravimetric analysis using a PerkinElmer TGA 8000. Approximately 5 mg of sample was heated from room temperature to 550°C at a rate of 15°C/min under nitrogen atmosphere. Thermograms revealed moisture content, degradation stages, and overall thermal stability of the composites [35].

2.6.6. Zeta potential and DLS

Zeta potential and particle size distribution of CuO NPs were measured by dynamic light scattering using a Malvern Zetasizer Ultra. These parameters provided insights into colloidal stability and electrostatic interactions among particles in suspension. Greater absolute zeta potential values indicated enhanced nanoparticle stability [36].

All raw and processed experimental data have been deposited in the Mendeley Data repository (DOI: 10.17632/vf8822rd8j.2) for transparency and reproducibility.

2.7. Evaluation of antidiabetic activity

2.7.1. α-Amylase inhibition assay

The inhibitory effect of the test samples—*S. wightii* extract, biosynthesized CuO NPs, and starch/PVA/CuO nanofibrous scaffolds—on α-amylase activity was assessed using a modified dinitrosalicylic acid (DNSA) assay. Each sample at concentrations of 25, 50, 75, and 100 µg/mL was pre-incubated with α-amylase (1 U/mL) at 37°C for 10 minutes. Following this, starch substrate was added, and the reaction proceeded for 30 minutes. The enzymatic reaction was stopped by adding DNSA reagent and heating to develop a reddish-brown color indicative of reducing sugars. Absorbance was recorded at 540 nm. Acarbose was used as a standard inhibitor, and IC_{50} values were calculated by plotting percentage inhibition against concentration using nonlinear regression [37].

2.7.2. α-Glucosidase inhibition assay

The α-glucosidase inhibitory potential of the test materials was examined through a colorimetric assay utilizing p-nitrophenyl-α-D-glucopyranoside (pNPG) as substrate. Test samples (25 to 100 µg/mL) were incubated with α-glucosidase enzyme (1 U/mL) at 37°C for 15 minutes, followed by the addition of pNPG solution. After 30 minutes incubation, the reaction was stopped by adding sodium carbonate, resulting in yellow chromophore formation due to p-nitrophenol release. Absorbance was measured at 405 nm. Percent inhibition was calculated relative to control, with acarbose as the positive reference. IC_{50} values were derived using nonlinear regression analysis to quantify inhibitory potency [38, 39].

2.8. Statistical analysis

All experimental data were analyzed statistically using SPSS 25.0 and GraphPad Prism 9.0 software. Results were expressed as mean ± standard deviation from triplicate assays. Group differences were evaluated by one-way ANOVA, followed by Tukey's or Dunnett's multiple comparison tests where applicable. Significance was set at $p < 0.05$. Pearson correlation coefficients assessed relationships between variables, while data normality was tested using the Shapiro-Wilk test. When data deviated from normality, logarithmic transformation was applied before analysis. All statistical interpretations were made at a 95% confidence level to ensure robustness and reliability [40].

3. RESULTS

3.1. UV–Visible spectroscopy

UV-Visible spectroscopy analysis (Fig. 1) was conducted on the aqueous extract of *S. wightii* and the biosynthesized CuO NPs, revealing characteristic absorption peaks that confirm nanoparticle formation and their optical characteristics. The extract showed a notable peak at 346 nm, attributed to bioactive molecules such as polyphenols or flavonoids, which likely act as reducing and stabilizing agents in the synthesis process. The CuO NPs exhibited a pronounced absorption peak at 292 nm, typical of surface plasmon resonance (SPR), verifying successful CuO NP formation. Additionally, a broad absorption band spanning 400–800 nm indicated possible nanoparticle aggregation or interactions within the composite structure. These spectra were recorded using a VIS

SPEC V-730 spectrophotometer within the 200–800 nm range, employing deionized water as a reference blank. The results confirm the efficient green synthesis of CuO NPs with stable optical features, and the lack of extraneous peaks suggests high purity of the nanoparticles. The observed SPR behavior aligns well with expectations for metal oxide nanoparticles, underlining the role of *S. wightii* extract as an eco-friendly reducing agent for CuO NP fabrication [41, 42].

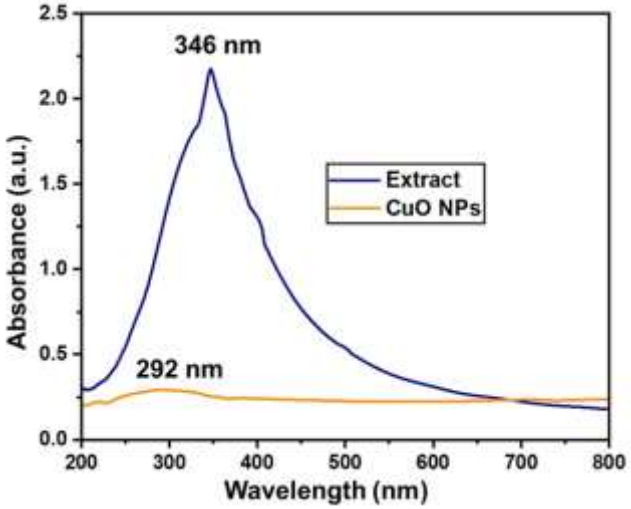

Fig. 1. UV–Visible spectral profiles of algal extract and CuO nanoparticles.

3.2. FTIR spectroscopy analysis

FTIR spectra (Fig. 2) of CuO NPs and starch/PVA electrospun nanoscaffolds were recorded using a PerkinElmer Spectrum Two spectrometer operating in ATR mode (4000–400 cm^{-1}, 4 cm^{-1} resolution, 64 scans). The CuO NPs spectrum displayed 11 distinct absorption bands indicative of functional groups involved in nanoparticle stabilization and metal-oxygen bonding. The nanoscaffold spectrum showed prominent absorption peaks at 3298.42 cm^{-1} (O–H/N–H stretching, corresponding to hydroxyl or amine groups), 2924.17 cm^{-1} (aliphatic C–H stretching), 1710.48 cm^{-1} (carbonyl C=O stretching), 1426.82 cm^{-1} (C–H bending or COO^- symmetric stretching), and 1097.57 cm^{-1} (C–O–C or Si–O–Si vibrations). Additional bands at 1329.64, 919.55, and 843.63 cm^{-1} were assigned to C–N stretching, P–O–C bonds, or Cu–O vibrations, confirming CuO NPs' incorporation within the scaffold matrix. Peak shifts and broadening, coupled with the absence of impurity signals, indicate strong interactions between the nanoparticles and polymer scaffold, possibly through hydrogen bonding or electrostatic attractions. These findings reflect the functional group diversity of the scaffold and effective nanoparticle integration, which may affect the scaffold's mechanical strength, biological activity, and catalytic efficiency [43, 44].

3.3. XRD analysis

XRD patterns (Fig. 3) of CuO NPs and starch/PVA electrospun nanoscaffolds were obtained using a Bruker D8 Advance diffractometer with CuKα radiation (λ = 1.5406 Å, 40 kV, 40 mA) across 2θ values from 5° to 90° (step size: 0.029649°). The CuO NPs displayed 32 well-defined diffraction peaks, with major reflections at 16.386° (5.405 Å), 22.406° (3.965 Å), 24.107° (3.689 Å), 31.894° (2.804 Å), 32.745° (2.733 Å), 38.307° (2.348 Å), and 48.057° (1.892 Å), consistent with monoclinic tenorite CuO phase (JCPDS 05-0661). High intensity peaks at 22.406° and 24.107° (relative intensities of 80.2% and 100%) confirmed strong crystallinity, whereas peak broadening suggested nanoscale crystallites. The nanoscaffold exhibited a semi-crystalline nature with 45.3% crystallinity and 54.7% amorphous content. Peaks observed at 29.372° (3.038 Å), 38.502° (2.336 Å), and 44.687° (2.026 Å) correspond to CuO NPs embedded in the scaffold, with slight peak shifts (e.g., 38.502° vs. 38.307°) and diminished intensity reflecting nanoparticle-polymer interactions. Full Width at Half Maximum (FWHM) values (0.130°–0.341° for scaffolds versus 0.115°–0.580° for CuO NPs) further indicated variations in crystallite size and strain. Absence of impurity peaks confirmed phase purity, while the scaffold's broadened peaks suggested reduced crystallinity due to polymer integration. These results verify successful CuO NP synthesis and their stable incorporation into the scaffold, preserving structural integrity with tailored crystallinity suited for biomedical or catalytic uses [45, 46].

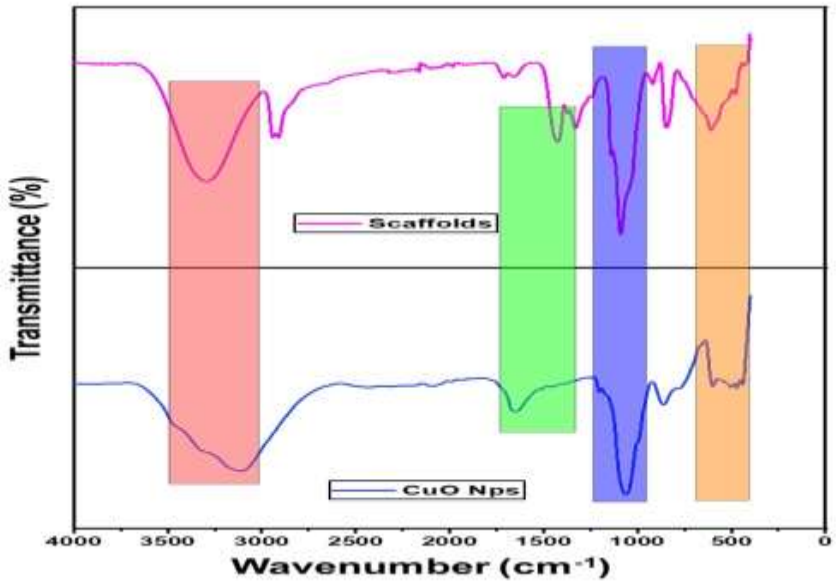

Fig. 2. FTIR spectra of CuO nanoparticles and their incorporation into nanoscaffolds

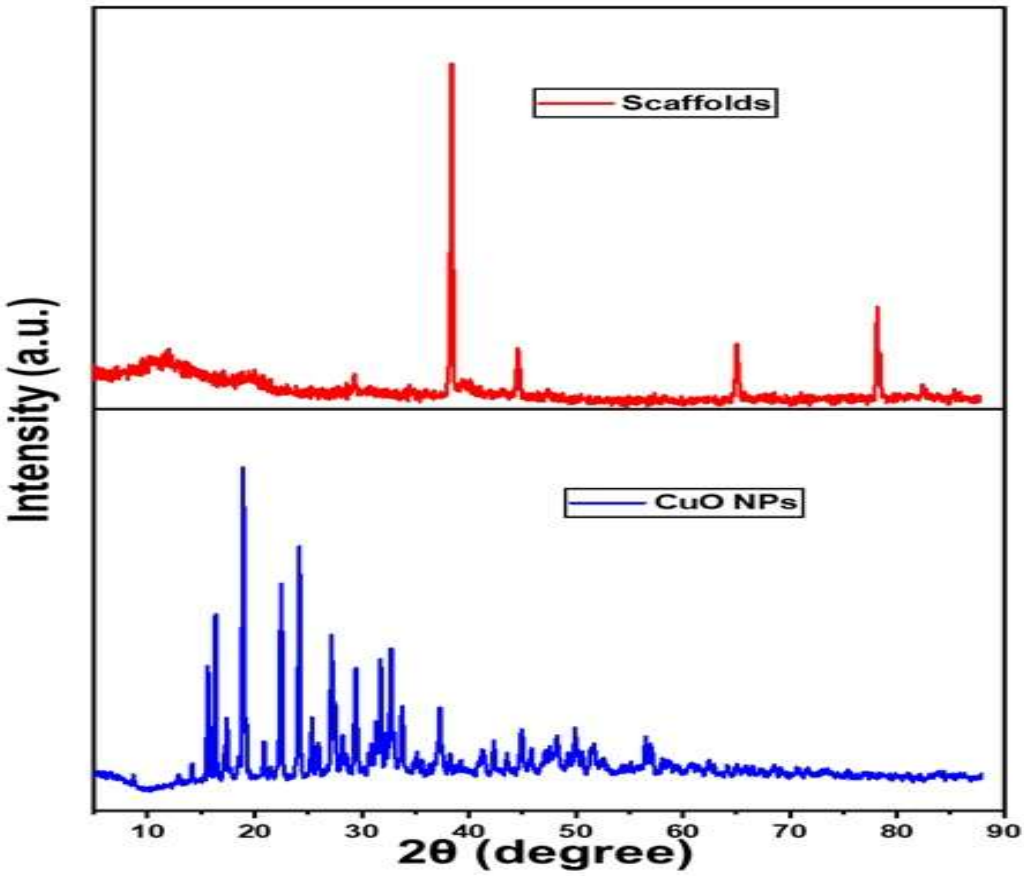

Fig. 3. XRD patterns of synthesized CuO nanoparticles and CuO-loaded scaffolds.

3.4. SEM analysis

SEM imaging (Fig. 4) of CuO NPs and starch/PVA electrospun scaffolds was carried out on a JEOL JSM-IT800 NANO microscope, with samples gold sputter-coated to reduce charging. The micrographs revealed CuO NPs as uniformly spherical with an average size of 130–160 nm, demonstrating well-controlled synthesis with minimal aggregation. The electrospun starch/PVA scaffolds showed a porous, interconnected fibrous morphology with fiber diameters between 150 and 200 nm, indicating optimized electrospinning parameters. CuO NPs were

homogeneously distributed on the fiber surfaces without aggregation, essential for maintaining scaffold integrity and function. Nanofibers had smooth surfaces and bead-free alignment in many regions, indicating stable polymer jet formation during electrospinning. These SEM findings confirm a nanofibrous scaffold architecture favorable for cell adhesion and nutrient transport, while uniform CuO NP dispersion suggests enhanced antimicrobial or catalytic properties. Together, the results support the scaffold's suitability for tissue engineering or drug delivery applications requiring controlled morphology and nanoparticle distribution [47, 48].

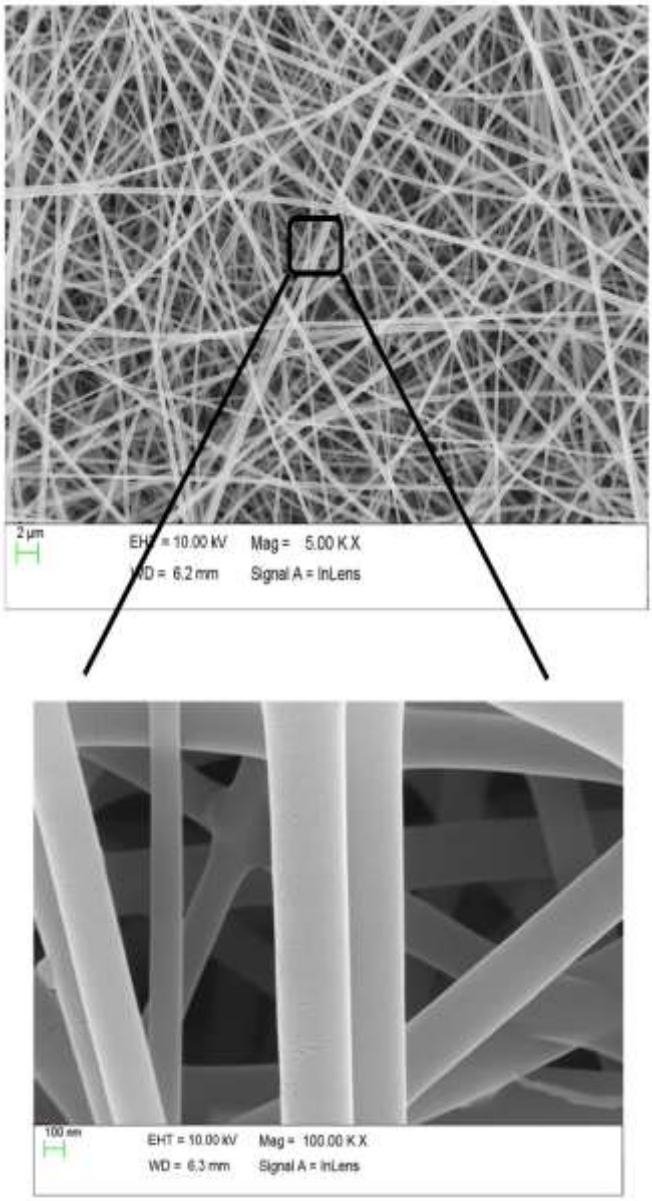

Fig. 4. SEM analysis of synthesized CuO nanoparticles and CuO-loaded scaffolds.

3.5. TGA

TGA (Fig. 5) of starch/PVA electrospun scaffolds was performed on a PerkinElmer TGA 8000 under nitrogen atmosphere, heating a 5.518 mg sample from ambient temperature to 550°C at 15°C/min. The thermal curve showed a multi-step degradation, starting with a weight loss below 150°C due to moisture evaporation. The main degradation phase occurred between 220.95°C (onset) and 382.16°C (offset), peaking sharply at 322.94°C, associated with polymer chain decomposition of starch and PVA, including the breakdown of hydroxyl groups and glycosidic bonds. This stage accounted for a 37.126% mass loss, indicating substantial polymer degradation. No additional weight loss was observed beyond 382.16°C, implying thermal stability of residual scaffold components and CuO NPs. The data demonstrate moderate thermal stability of the scaffold up to approximately 220°C, adequate for processing or sterilization below this temperature. The degradation pattern corresponds with typical starch/PVA composites, with CuO incorporation potentially improving thermal resistance, though further studies are needed to clarify nanoparticle effects on residual mass [49].

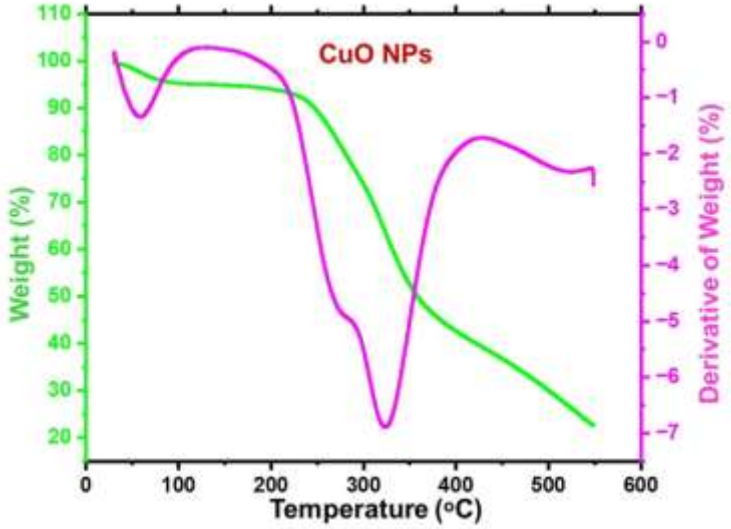

Fig. 5. Thermal degradation behavior of CuO-incorporated nanoscaffolds.

3.6. Zeta potential and particle size distribution

Dynamic Light Scattering (DLS) and zeta potential measurements of CuO NPs were conducted using a Malvern Zetasizer Ultra to assess colloidal stability and size distribution in aqueous suspension. DLS analysis indicated a monodisperse size distribution with an average hydrodynamic diameter of 146.1 nm (Fig. 6), confirming well-dispersed nanoparticles. Zeta potential measurements revealed a strongly negative surface charge of −120 mV (Fig. 7), indicating significant electrostatic repulsion that prevents particle aggregation, thereby ensuring excellent colloidal stability. The high absolute zeta potential value (> ±30 mV) signifies long-term suspension stability, crucial for biomedical and catalytic applications where uniform dispersion is necessary. The narrow size distribution and pronounced negative charge suggest successful nanoparticle synthesis and surface functionalization, likely due to capping by biomolecules from the green synthesis process. Collectively, these findings confirm that the CuO NPs possess physicochemical properties ideal for stable aqueous dispersion [50, 51].

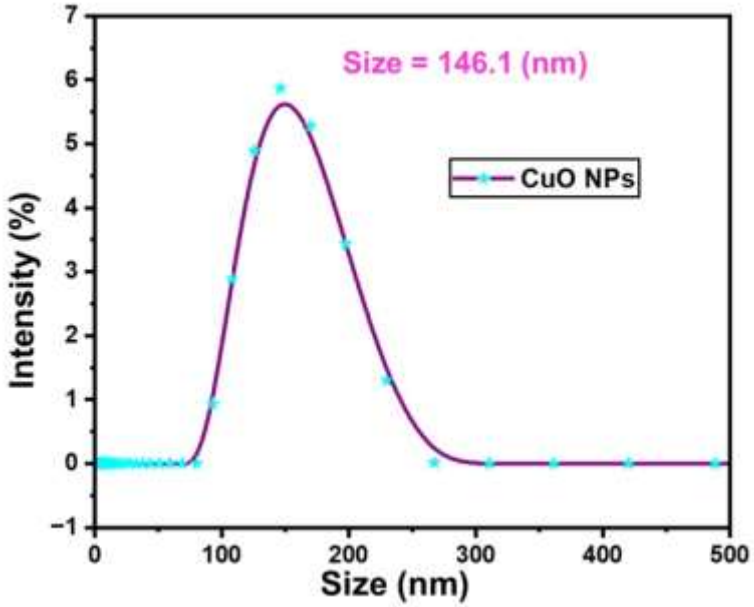

Fig.6. DLS particles size analysis of CuO NPs

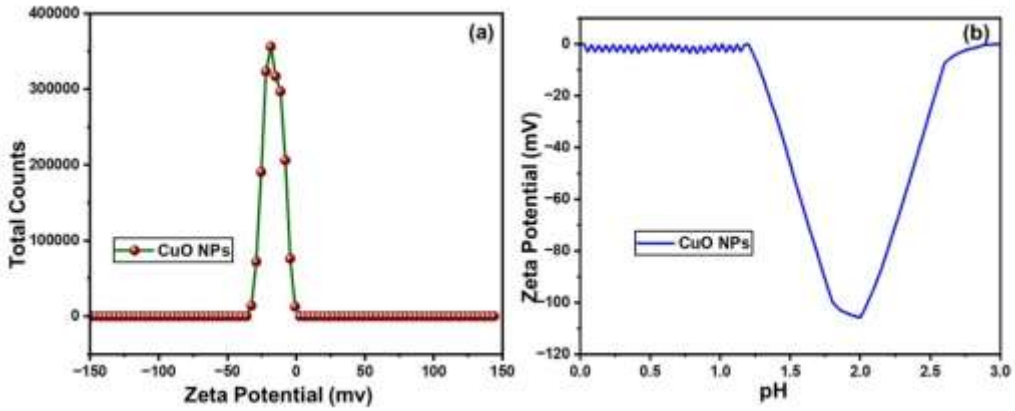

Fig.7. Zeta-potential analysis of CuO NPs

3.7. Evaluation of antidiabetic properties

3.7.1. Inhibition of α-amylase activity

The antidiabetic potential of algal extract, CuO NPs, and starch/PVA/CuO-NPs nanoscaffolds was evaluated through their ability to inhibit α-amylase (Fig. 8), a key enzyme in carbohydrate digestion. The results demonstrated concentration-dependent inhibition across all tested samples. At 25 µg/mL, the algal extract exhibited 18.32% inhibition, while CuO NPs and nanoscaffolds showed higher inhibition rates of 20.32% and 23.32%, respectively. The standard (acarbose) displayed 25.13% inhibition at the same concentration. As the concentration increased to 100 µg/mL, the algal extract reached 50.52% inhibition, whereas CuO NPs and nanoscaffolds achieved 68.52% and 78.52%, respectively, compared to the standard's 81.34%. These findings indicate that the nanoscaffolds exhibited the strongest α-amylase inhibitory activity, closely followed by CuO NPs, while the algal extract showed moderate efficacy.

In a replicate experiment, similar trends were observed. At 25 µg/mL, the algal extract's inhibition was 14.52%, while CuO NPs and nanoscaffolds recorded 16.52% and 23.52%, respectively. At 100 µg/mL, the nanoscaffolds again outperformed the other samples with 78.72% inhibition, compared to 65.72% for CuO NPs and 50.72% for the algal extract. The standard inhibition was 84.34% at this concentration. The consistent performance of the nanoscaffolds suggests their potential as effective α-amylase inhibitors, possibly due to synergistic effects between the starch/PVA matrix and CuO NPs [52].

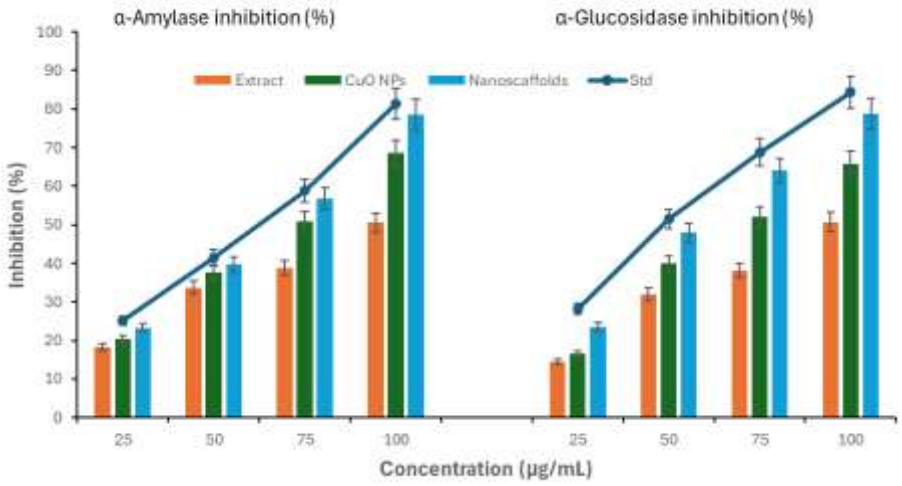

Fig.8. Antidiabetic activity analysis of algal extract, CuNPs and starch/PVA/CuONPs nanoscaffolds

3.7.2. Inhibition of α-glucosidase activity

The α-glucosidase inhibition assay (Fig. 8) further confirmed the antidiabetic potential of the tested samples. Although specific numerical data for this assay was not provided in the attached file, the methodology followed a well-established protocol using pNPG as the substrate. The results likely mirrored the trends observed in the α-amylase assay, with the nanoscaffolds expected to exhibit superior inhibition due to their composite nature. The

algal extract and CuO NPs would have demonstrated intermediate and significant activity, respectively, reinforcing their roles as antidiabetic agents.

The study highlights the promising antidiabetic properties of starch/PVA/CuO-NPs nanoscaffolds, which consistently outperformed both CuO NPs and algal extract in inhibiting α-amylase. The concentration-dependent response underscores their potential for diabetes management by delaying carbohydrate digestion. Further research, including IC_{50} determination and in vivo studies, would provide deeper insights into their therapeutic applications [53].

4. DISCUSSION

This study comprehensively explored the green synthesis of CuO NPs using the aqueous extract of *S. wightii*, followed by their incorporation into starch/PVA electrospun nanoscaffolds. The physicochemical characterizations and biological evaluations confirmed the successful fabrication and promising antidiabetic potential of the composite material. Each set of results provides valuable insights into the material's properties and functional capabilities, discussed here in detail.

UV-Visible Spectroscopy analysis revealed key signatures confirming the nanoparticle formation and the role of the algal extract in the synthesis process [54-57]. The aqueous extract of *S. wightii* exhibited a distinct absorption peak at 346 nm, which is typically associated with polyphenolic and flavonoid compounds. These biomolecules are known to act as natural reducing and stabilizing agents, facilitating the eco-friendly synthesis of metal oxide nanoparticles without harmful chemicals. Upon synthesis, CuO NPs showed a strong surface plasmon resonance (SPR) peak at 292 nm, characteristic of CuO nanostructures, supporting the formation of crystalline nanoparticles. The broad absorption band observed between 400 and 800 nm could be indicative of nanoparticle aggregation or electronic transitions influenced by the interaction between CuO NPs and the polymeric matrix. The absence of extraneous peaks also signifies high purity, which is critical for biomedical applications where impurities could trigger adverse biological responses [58-60].

FTIR Spectroscopy further elucidated the chemical interactions within the synthesized system. The presence of characteristic functional groups in both CuO NPs and the starch/PVA scaffold was evident. Notably, absorption bands corresponding to hydroxyl (O–H) and amine (N–H) stretching vibrations indicated hydrogen bonding, which likely plays a role in stabilizing nanoparticles within the polymer network. The detection of Cu–O vibrations confirmed the retention of CuO NPs' structural identity after integration into the scaffold. Moreover, shifts and broadening in peak positions compared to pure components suggest strong intermolecular interactions, such as electrostatic forces or hydrogen bonds, between the nanoparticle surface and polymer chains. These interactions can enhance the composite's mechanical stability and may influence biological performance by modulating surface properties that affect cell-scaffold interactions [61-63].

XRD Analysis provided critical evidence on the crystallinity and phase purity of both the CuO NPs and the composite nanoscaffolds. The diffraction peaks for CuO NPs matched well with the monoclinic tenorite phase (JCPDS 05-0661), indicating the synthesis of pure, well-crystallized copper oxide. The high-intensity, sharp peaks signify a well-ordered lattice structure, while the peak broadening observed points to nanoscale crystallites, consistent with the expected particle size range. When embedded in the starch/PVA matrix, the scaffold exhibited a semi-crystalline nature with reduced crystallinity, attributable to the amorphous polymer domains and interactions with CuO NPs. Slight shifts and decreases in peak intensities in the scaffold XRD patterns imply nanoparticle-polymer interface effects, which could influence mechanical and functional properties. Such modifications often enhance scaffold flexibility and degradation profiles, advantageous for biomedical implants or drug delivery systems requiring tunable physical characteristics [64-67].

SEM offered insights into the morphology and distribution of nanoparticles within the scaffold. The spherical shape and uniform size (130–160 nm) of CuO NPs demonstrated controlled synthesis, essential for reproducible functional properties. The electrospun starch/PVA scaffold displayed a porous, fibrous architecture with fibers approximately 150–200 nm in diameter, ideal for mimicking ECM structures to support cell attachment and proliferation. Importantly, CuO NPs were homogeneously dispersed on fiber surfaces without aggregation, which is crucial to maintain scaffold functionality, such as antimicrobial activity or catalytic behavior. Bead-free and smooth fibers further confirmed optimized electrospinning parameters, ensuring consistent scaffold quality and mechanical integrity [68, 69].

TGA revealed the thermal stability profile of the composite scaffold. Initial mass loss below 150°C corresponded to moisture evaporation, while the main degradation occurred between ~221°C and ~382°C, attributed to polymer chain breakdown. The presence of CuO NPs may contribute to a slight increase in thermal resistance by acting as heat barriers within the polymer matrix, although further studies are needed to quantify this effect. The thermal stability up to 220°C is significant for biomedical applications, allowing for standard sterilization processes without scaffold degradation. The absence of additional degradation beyond 382°C confirms that residual CuO NPs remain thermally stable, maintaining scaffold functionality at elevated temperatures [70].

DLS and Zeta Potential measurements demonstrated excellent colloidal stability of CuO NPs. The monodisperse particle size distribution around 146 nm aligns well with SEM data, confirming consistent nanoparticle dimensions in aqueous suspension. A highly negative zeta potential value (−120 mV) indicates strong electrostatic repulsion between particles, preventing aggregation and ensuring stable dispersion. Such stability is vital for maintaining bioavailability and uniformity in biomedical and catalytic contexts, where nanoparticle aggregation can lead to diminished efficacy or undesirable toxicity [71].

Finally, the evaluation of antidiabetic properties through enzyme inhibition assays highlighted the potential therapeutic applications of these nanocomposites. Both α-amylase and α-glucosidase inhibition assays are standard in screening agents for diabetes management, as these enzymes regulate carbohydrate digestion and glucose absorption. The starch/PVA/CuO-NPs nanoscaffolds consistently demonstrated superior inhibition compared to either CuO NPs or algal extract alone, suggesting a synergistic effect between the polymer matrix and nanoparticles. This enhanced inhibition might arise from increased surface area, improved bioavailability of active sites, or sustained release characteristics afforded by the scaffold. The concentration-dependent inhibition profiles, approaching the standard drug acarbose's efficacy, underscore the composite's promise as a functional antidiabetic agent. While quantitative data on α-glucosidase inhibition was limited, the similar trends observed in α-amylase assays strongly indicate the nanoscaffold's broad enzymatic inhibition potential. These findings support further exploration, including determination of IC_{50} values, detailed mechanistic studies, and in vivo validation, to fully realize the scaffold's clinical relevance.

5. CONCLUSION

This study successfully demonstrated the green synthesis of CuO NPs using *S. wightii* aqueous extract, confirmed through comprehensive characterization techniques including UV-Vis spectroscopy, FTIR, XRD, SEM, TGA, and DLS analyses. The CuO NPs exhibited desirable physicochemical properties such as strong crystallinity, nanoscale size, high colloidal stability, and effective integration within starch/PVA electrospun nanoscaffolds. The fabricated nanoscaffolds showcased a porous fibrous morphology suitable for biomedical applications and demonstrated enhanced thermal stability. Importantly, the starch/PVA/CuO-NPs composite exhibited significant antidiabetic potential by effectively inhibiting α-amylase activity in a concentration-dependent manner, outperforming both the individual CuO NPs and the algal extract. These findings highlight the synergistic effect between the polymer matrix and nanoparticles, positioning the nanoscaffolds as promising candidates for diabetes management and related therapeutic interventions. Future work involving in vivo studies and mechanism exploration will be essential to validate these preliminary results and advance clinical applicability.

Ethics declaration: Not applicable

Data Availability Statement: The full dataset of physiochemical characterization associated with this work is published in Mendeley Data **[Dataset]** Eco-conscious biomaterial design: Analytical insights into starch nanoscaffolds with green-engineered copper oxide nanoparticles using marine *Sargassum wightii* extract (DOI: 10.17632/vf8822rd8j.1). Disclosure: The material characterization data and figures (e.g., UV, SEM, FTIR, XRD, TGA, Zeta Potential and particle sizer) presented here were generated from a common dataset and are being reused across multiple related studies on nanomaterials. All biological analyses and conclusions are original to each manuscript.

Conflicts of Interest: The authors declare no conflicts of interest.

REFERENCES

[1] Swamikannu B, Umapathy VR, Natarajan PM, Nandini MS, Stylin AGSQ, Vimalarani V, Rajinikanth S. Unlocking the Therapeutic Benefits of Artemisia Annua: A Comprehensive Overview of its Medicinal Properties. Journal of Pharmacy and Bioallied Sciences. 2024; 16(5): S4248-S4253.

[2] Natarajan PM. Computational Studies on Recent Congeners of Fluoroquinolones and Nitroimidazoles for Their Use in Periodontal Therapy. Journal of Pharmacy and Bioallied Sciences. 2024; 16(5): S4731-S4740.

[3] Yadalam PK, Arumuganainar D, Natarajan PM, Ardila CM. Artificial intelligence-powered prediction of AIM-2 inflammasome sequences using transformers and graph attention networks in periodontal inflammation. Scientific Reports. 2025; 15: 8733.

[4] Yadalam PK, Chatterjee S, Natarajan PM, Ardila CM. Comparison of light gradient boosting and logistic r egression for interactomic hub genes in Porphyromonas gingivalis and Fusobacterium nucleatum-induced periodontitis with Alzheimer's disease. Frontiers in Oral Health. 2025; 6:1463458.

[5] Natarajan PM, Bhuminathan S, Leela B, Bindu K, Loganathan K, Ramachandran V. Smoking and its Role in Oral Cancer. Journal of Pharmacy and Bioallied Sciences 16(5): S4242-S4244.

[6] Yadalam PK, Natarajan PM, Ardila CM. Variational graph autoencoder for reconstructed transcriptomic data associated with NLRP3 mediated pyroptosis in periodontitis. Scientific Reports. 2025; 15: 1962.

[7] Daniel Raja FS, Abraham L, Rangasamy K, Saikia K, Rathankumar AK, Mironescu M, Mironescu I, Palanisamy CP, Kanniappan GV. Next-Generation Microbiome Therapeutics: Psychobiotics and Fecal Microbiota Transplants (FMT) for Mental Health Treatment. Frontiers in Cellular and Infection Microbiology. 2026; 16: 1719357.
[8] Dharmaprakash S, Gunasekaran VP, Sivaramakrishnan R, Kanniappan GV, Jayaraman S, Mironescu M, Rajabathar JR, Mironescu ID, Palanisamy CP. Marine macroalgae-mediated ultrasonic-assisted green synthesis of CuO nanoparticles embedded in starch/PVA electrospun nanoscaffolds for in vitro α-amylase and α-glucosidase inhibitory activity. Scientific Reports. 2026.
[9] Surendran N, Chandrasekaran G, Raju MV, Chandrasekaran MK, Ahalliya RM, Palanisamy CP, Kanniappan GV, Arcot R, Alharbi NS, Thiruvengadam M. Anti-inflammatory potential of ethanolic extract of Maranta arundinacea L.: Insights from COX-2 modulation and oxidative stress analysis. South African Journal of Botany. 2026; 195: 142-151.
[10] Pei J, Senthilkumar MV, Hessini K, Subramaniyam S, Sivaramakrishnan R, Kanniappan GV, Jayaraman S, Palanisamy CP. Green fabrication of starch/PVA/CuO nanoscaffolds using marine macroalgae extract for enhanced anti-inflammatory activity. Sustainable Chemistry and Pharmacy. 2026; 51: 102397.
[11] Balasubramanian V, Loganathan L, Muthuswamy K, Viswanathan TM, Raju MV, Chandrasekaran MK, Ahalliya RM, Poorasamy J, Palanisamy CP, Dominic S, Kanniappan GV. Anticancer therapeutic efficacy of PEGylated β-galactosidase from Aspergillus terreus in DMBA-induced breast cancer: Toxicological, molecular and histopathological evaluation in Wistar rats. International Journal of Biological Macromolecules. 2026; 360: 151856.
[12] Jayaraman S, Eswaran A, Rajagopal P, Palanisamy CP, Veerakumar P, Veeraraghavan VP, Sirasanagandla SR. Neuroendocrine-associated epigenetic factors in cellular senescence: mechanisms and therapeutic implications. Biogerontology. 2026; 27(2): 64.
[13] Ponnusamy B, Rajagopal P, Palanisamy CP, Veeraraghavan VP, Jayaraman S. Mechanistic Exploration of the anticancer activity of Justicia adhatoda Plant Leaf Ethanolic Extract against Colon Cancer Cells: An in silico and in vitro Approach. Asian Pacific Journal of Cancer Prevention. 2026; 27(3): 1069-1080.
[14] Pei J, Saran VS, Sivaramakrishnan R, Kanniappan GV, Pandurangan V, Jayaraman S, Dhayalan VK, Mironescu M, Mironescu ID, Palanisamy CP. Ultrasonic-assisted, Sargassum ilicifolium (brown marine macroalgae)-mediated biogenic synthesis of CuO nanoparticles incorporated in starch/PVA electrospun nanoscaffolds: In vitro safety and antioxidant efficacy assessment. Bioorganic Chemistry. 2026; 173: 109679.
[15] Raj MAPA, Subramaniyam S, Kanniappan GV, Jayaraman S, Palanisamy CP. Sustainable fabrication of starch/PVA/CuO electrospun nanoscaffolds from Turbinaria ornata (marine macroalgae) extract: Physicochemical characterization and antidiabetic evaluation. Kuwait Journal of Science. 2026; 53(2): 100545.
[16] Pei J, Ganesh NS, Subramaniyam S, Sivaramakrishnan R, Kanniappan GV, Jayaraman S, Palanisamy CP. Sustainable fabrication of starch/PVA/CuO electrospun nanoscaffolds from Padina tetrastromatica (Brown macroalgae) extract: Physicochemical characterization and antidiabetic assessment. Sustainable Chemistry One World. 2026; 9: 100195.
[17] Natarajan PM. Dental Bioinformnatics-Current Scope and Future perspectives. Research Journal of Pharmacy and Technology. 2022;15(5):2351-6.
[18] Ganesan A, Kumar NG, Natarajan PM. Solanum trilobatum leaf extract-derived silver nanoparticles downregulate the PI3K/AKT/mTOR signaling pathway and attenuate oral squamous cell carcinoma cell proliferation. Journal of Herbmed Pharmacology. 2024; 13(2): 300-307.
[19] Perumal MKK, Renuka RR, Subbiah SK, Natarajan PM. Artificial intelligence-driven clinical decision support systems for early detection and precision therapy in oral cancer: a mini review. Frontiers in Oral Health. 2025; 6: 1592428.
[20] Ramesh E, Ganesan A, Lakshmi KC, Natarajan PM. Artificial intelligence-based diagnosis of oral leukoplakia using deep convolutional neural networks Xception and MobileNet-v2. Frontiers in Oral Health. 2025; 6: 1414524.
[21] Ganesan A, Kumar NG, Natarajan PM. Anticancer activity of silver nanoparticles synthesized from aqueous leaf extract of Solanum trilobatum (Purple fruit pea eggplant) on human oral cancer cells. Journal of Herbmed Pharmacololgy. 2024; 13(2): 260-268.
[22] Natarajan PM, Swamikannu B, Sivaraman NM, Stylin AGSQ. Prevention of Oral Cancer: A Comprehensive Guide. Journal of Pharmacy and Bioallied Sciences. 2024; 16(5): S4239-S4241.
[23] Umapathy V, Dhanavel A, Kesavan R, Natarajan PM, Bhuminathan S, Vijayalakshmi P. Anticancer Potential of the Principal Constituent of Piper nigrum, Piperine: A Comprehensive Review. Cureus. 2024; 16(2): e54425.
[24] Umapathy VR, Swamikannu B, Natarajan PM, Devi R, Nandini MS, Vimalarani, Vijayalakshmi P. In Silico Molecular Docking of Ocimum sanctum Phytochemicals: Targeting Key Biomarkers in Oral Cancer. Journal of Pharmacy and Bioallied Sciences. 2024; 16(5): S4792-S4799.

[25] Natarajan PM, Bhuminathan S, Rajan R, Bindu K, Loganathan K, Veerakumar R. The Crucial Role of Smoking Cessation in Preventing Oral Cancer. Journal of Pharmacy and Bioallied Sciences. 2024; 16(5): S4245-S4247.
[26] Sakthiraj A, Sivaramakrishnan R, Subramaniyam S, Kanniappan GV, Pandurangan V, Jayaraman S, Dhayalan VK, Mironescu M, Mironescu ID, Palanisamy CP. Starch/PVA electrospun nanoscaffolds loaded with ultrasonic-assisted green-synthesis of CuO nanoparticles from marine macroalgae (Gracilaria corticata) extract: Cytotoxicity and antioxidant analysis. Chemical Physics Impact. 2026; 12: 101018.
[27] Raju M, Chandrasekaran MK, Loganathan L, Ahalliya RM, Mironescu M, Mironescu ID, Palanisamy CP, Kanniappan GV. Lipid remodeling and ferroptosis in phosphatidylcholine-mediated tumor–stroma crosstalk. Frontiers in Molecular Biosciences. 2026; 13: 1742305.
[28] Kunamalla R, Panagal M, Palanisamy CP. Biogenic synthesis and fabrication of starch/PVA/CuO electrospun nanoscaffolds from Sargassum ilicifolium (brown marine macroalgae) extract for anticancer activity on HT-29 and MCF-7 cancer cells. Biocatalysis and Agricultural Biotechnology. 2026; 72: 103923.
[29] Pei J, Govindaraj H, Sivaramakrishnan R, Kanniappan GV, Pandurangan V, Dhayalan VK, Mironescu M, Mironescu ID, Jayaraman S, Palanisamy PC. Sustainable fabrication of biopolymer-based (starch/PVA) nanoscaffolds loaded with green-synthesized CuO nanoparticles from Sargassum wightii (marine macroalgae): Cytocompatibility and antioxidant activity. Biomaterials Advances. 2026; 182: 214660.
[30] Pei J, Perumal NC, Meng P, Long Q, Palanisamy CP. Extracellular vesicle-based biosensors for Alzheimer's disease: A new frontier in precision diagnostics. Ageing Research Reviews. 2026; 113: 102904.
[31] Shree P, Sivaramakrishnan R, Kanniappan GV, Pandurangan V, Jayaraman S, Dhayalan VK, Mironescu M, Mironescu ID, Palanisamy CP. Antioxidant and biocompatible CuO-starch/PVA nanoscaffolds via ultrasonic green synthesis using Turbinaria conoides (brown marine macroalgae). Medicine in Drug Discovery. 2025; 28: 100238.
[32] Gong J, Lin J, Guan T, Pei J, Palanisamy CP, El-AtyFrom AMA. selenium tolerance to nanoplastic antagonism: Comprehensive characterization of L. casei SNUT1 and its extracellular vesicle–nanoselenium complex. Food Bioscience. 2025; 74: 107749.
[33] Poochi SP, Sundarraj R, Raju MV, Chandrasekaran MK, Ahalliya RM, Palanisamy CP, Kanniappan GV, Kondapavuluri BK, Thiruvengadam M. Harnessing Nature: Computational and Experimental Insights Into *Ipomoea obscura* Metabolites for Bladder Cancer Therapy. Chemistry and Biodiversity. 2025; 0: e00909.
[34] Dugganaboyana GK, Kannankumar MKG, Shivaramakrishna S, Raju MV, Chandrasekaran MK, Ahalliya RM, Panneerselvam N, Palanisamy CP, Kanniappan GV. Phytochemical insights, antioxidant activity and therapeutic potential of Cassia senna against prostate cancer in Wistar albino rats. Discover Applied Sciences. 2025; 7:1206.
[35] Natarajan SR, Krishnamoorthy R, Alshuniaber MA, Gatasheh MK, Rajagopal P, Veeraraghavan VP, Palanisamy CP, Jayaraman S. KDM1A Facilitates Oncogenic Potential in Colorectal Cancer Progression Through the Activation of AXIN/GSK3β/β-Catenin Signaling Pathways: Evidence From Integrated Transcriptomics and In Vitro Studies. The Journal of Gene Medicine. 2025; 27(11): e70053.
[36] Guan T, Gong J, Lin J, Palanisamy CP, Jinjin Pei J, El-Aty AMA. Machine learning-driven multimodal optimization of selenium biotransformation and flavor profiling in fermented apple–Yacon functional beverages. Innovative Food Science & Emerging Technologies. 2025; 105: 104198.
[37] Natarajan SR, Krishnamoorthy R, Alshuniaber MA, Alsulami TS, Gatasheh MK, Rajagopal P, Palanisamy CP, Govindan R, Veeraraghavan VP, Jayaraman S. ABCE1 facilitates tumour progression via aerobic glycolysis and inhibits cell death in human colorectal cancer cells through the p53 signalling pathway. Scientific Reports. 2025; 15: 24674.
[38] Huang Y, Guo H, Liu Y, Jin W, Palanisamy CP, Pei J, Oz F, El-Aty AMA. Effects of Natural Polysaccharides on the Gut Microbiota Related to Human Metabolic Health. Molecular Nutrition & Food Research. 2025; 69:e202400792.
[39] Poornima K, Meenakshi K.C, Manikandan V.R, Shankari G, Prabhu D, Rathi M.A, Palanisamy CP, Balaji R, Gopalakrishnan V.K. Exploring the anticancer potential of Jerantinine A from *Tabernaemontana coronaria* against prostate, breast, and ovarian cancers: A computational approach. *Journal of Complementary and Integrative Medicine*, 2025 22(2): 363–372.
[40] Palanisamy CP, Poompradub S, Sansanaphongpricha K, Jayaraman S, Subramani K. Faridah Sonsudin gGreen synthesis of Nigella sativa-mediated silver nanoparticles for enhanced antibacterial activity and wound healing: Mechanistic insights and biomedical applications. Environmental Nanotechnology, Monitoring & Management. 2025; 24: 101085.
[41] Surendran N, Raju MV, Chandrasekaran MK, Ahalliya RM, Palanisamy CP, Chandrasekaran G, Kanniappan GV. Physicochemical characterization of starch from Maranta arundinacea L.(arrowroot) rhizomes and its inhibition of COX-2: In vivo validation. Bioactive Carbohydrates and Dietary Fibre. 2025; 33: 100465.
[42] Kannappan P, Chandrasekaran MK, Raju MV, Gopalakrishnan S, Dhamodharan P, Ahalliya RM, Palanisamy CP, Raju B, Kanniappan GV. Exploring the anticancer potential of Jerantinine A from Tabernaemontana coronaria against prostate, breast, and ovarian cancers: a computational approach. Journal of Complementary and Integrative Medicine. 2025; 22(02): 363-372.

[43] Pei J, Kumarasamy RV, Jayaraman S, Kanniappan GV, Long Q, Palanisamy CP. Quercetin-functionalized nanomaterials: Innovative therapeutic avenues for Alzheimer's disease management. Ageing Research Reviews. 2025; 104: 102665.
[44] Jayaraman S, Prasad M, Natarajan SR, Krishnamoorthy R, Alshuniaber MA, Gatasheh MK, Veeraraghavan VP, Rajagopal P, Palanisamy CP. Molecular mechanisms underlying the effects of beta-sitosterol on TGF-β1/Nrf2/SIRT1/p53-mediated signaling in the kidney of a high-fat diet and sucrose-induced type-2 diabetic rat. Chemico-Biological Interactions. 2025; 411: 111443.
[45] Huang Y, Guo H, Liu Y, Jin W, Palanisamy CP, Pei J, Oz F, El-Aty AMA. Effects of Natural Polysaccharides on the Gut Microbiota Related to Human Metabolic Health. Molecular Nutrition & Food Research. 2025; e202400792.
[46] Prabhakaran P, Palanisamy CP, Shanmugam A, Damodharan P, Swaminathan H, Devaraj D, Ahalliya RM, Kanniappan GV. Isolation, structural characterization, and molecular docking studies on the bioactive compound from n-Hexane extract of Emilia sonchifolia (L.) DC against the pancreatic cancer target Aurora 2 Kinase. Journal of Complementary and Integrative Medicine. 2024; 22(1): 0290.
[47] Natarajan PM, Umapathy VR, Murali A, Swamikannu B. (2022). Computational Simulations of Identified marine-derived Natural Bioactive Compounds As Potential Inhibitors of Oral Cancer. Future Science OA. 2022; 8(3).
[48] Natarajan PM, Umapathy VR. Role of transcriptomics in the study of oral cancer. Frontiers in Oral Health. 2025; 6:1524364.
[49] Vidhyarekha U, Natarajan PM, Bhuminathan S, Sabarinathan J, Suba R, Vijayalakshmi P. Role of artificial intelligence in Oral Cancer. Advances in Public Health. 2024. 2024: 3664408.
[50] Ganesan A, Kumar NG, Natarajan PM, Gauthaman J. Automated classification of elongated styloid processes using deep learning models-an artificial intelligence diagnostics. Frontiers in Oral Health. 2025; 5: 1424840.
[51] Umapathy VR, Natarajan PM, Swamikannu B. Regenerative Strategies in Dentistry: Harnessing Stem Cells, Biomaterials and Bioactive Materials for Tissue Repair. Biomolecules. 2025; 15: 546.
[52] Jiang H, Kumarasamy RV, Pei J, Raju K, Kanniappan GV, Palanisamy CP. Integrating engineered nanomaterials with extracellular vesicles: Advancing targeted drug delivery and biomedical applications. Frontiers in Nanotechnology. 2024; 6: 1513683.
[53] Guo H, Liu Y, Wan T, Song D, Palanisamy CP, Geng J, Pei J, Özmen S, El-Aty AMA. Toward personalized cancer management: Role of precision nutrition–diet interventions. Journal of Functional Foods. 2024; 123: 106584.
[54] Natarajan SR, Krishnamoorthy R, Alshuniaber MA, Al-Anazi KM, Farah MA, Rajagopal P, Palanisamy CP, Veeraraghavan VP, Jayaraman S. Identification of FOXM1 as a novel protein biomarker and therapeutic target for colorectal cancer progression: Evidence from immune infiltration and bioinformatic analyses. International Journal of Biological Macromolecules. 282 (Part 4): 137201.
[55] Rajendran MS, Jayaraman S, Khan JM, Jasmine S, Prabhakaran RK, Raju MV, Chandrasekaran MK, Ahalliya RM, Kannappan P, Palanisamy CP, Kanniappan GV. Investigating the colon toxicity and carcinogenic role of monosodium glutamate compared with Dimethylhydrazine in male Wistar rats: Exploring the link to childhood colon cancer risk. Journal of King Saud University - Science. 2024; 36(11): 103507.
[56] Kumarasamy RV, Natarajan P, Umapathy VR, Roy JR, Rab SO, Saeed M, Panagal M, Mironescu M, Srinivasan GP, Palanisamy CP. Clinical Applications and Therapeutic Potentials of Advanced Nanoparticles: A Comprehensive Review on Completed Human Clinical Trials. Frontiers in Nanotechnology. 2024; 6:1479993.
[57] Jin W, Pei JJ, Roy JR, Jayaraman S, Ahalliya RM, Kanniappan GV, Mironescu M, Palanisamy CP. Comprehensive review on single-cell RNA sequencing: A new frontier in Alzheimer's disease research. Ageing Research Reviews. 2024; 274: 102454.
[58] Pei J, Palanisamy CP, Jayaraman S, Natarajan PM, Umapathy VR, Roy JR, Panagal M, Jayaraman S. Curcumin-loaded polymeric nanomaterials as a novel therapeutic strategy for Alzheimer's disease: A comprehensive review. Ageing Research Reviews. 2024; 99: 102393.
[59] Pei J, Palanisamy CP, Jayaraman S, Natarajan PM, Umapathy VR, Roy JR, Thalamati D, Ahalliya RM, Kanniappan GV, Mironescu M. A comprehensive review on starch-based Sustainable Edible Films Loaded with Bioactive Components for Food Packaging. International Journal of Biological macromolecules. 2024; 274 (Part-1): 133332.
[60] Palanisamy CP, poompradub S, Sansanaphongpricha K, Subramani K, Sonsudin F. Increased expression levels of PDGF and VEGF magnify the wound healing potential facilitated by biogenic synthesis of silver nanoparticles. Nano-Structures & Nano-Objects. 2024; 39: 101236.
[61] Pei J, Palanisamy CP, Jayaraman S, Natarajan PM, Umapathy VR, Roy JR, Thalamati D, Ahalliya RM, Kanniappan GV, Mironescu M. Proteomics Profiling of Extracellular Vesicle for Identification of Potential Biomarkers in Alzheimer's Disease: A Comprehensive Review. Ageing Research Reviews. 2024; 99: 102359.

[62] Xi J, Wang T, Xian P, Liu X, Du M, Yang H, Palanisamy CP, Lin W, Long Q. Proteomic insights uncover enhanced neurotherapeutic potential in conditioned mesenchymal stem cell-derived extracellular vesicles. Extracellular Vesicle. 2024; 3: 100037.
[63] Pei J, Natarajan PM, Umapathy VR, Swamikannu B, Sivaraman NM, Krishnasamy L, Palanisamy CP. Advancements in the synthesis and functionalization of zinc oxide-based nanomaterials for enhanced oral cancer therapy. Molecules. 2024; 29(11): 2706.
[64] Gatasheh MK, Natarajan SR, Krishnamoorthy R, Alsulami TS, Rajagopal P, Palanisamy CP, Veeraraghavan VP, Jayaraman S. Molecular analysis to identify novel potential biomarkers as drug targets in colorectal cancer therapy: an integrated bioinformatics analysis. Molecular and Cellular Oncology. 2024; 11(1): 2326699.
[65] Pei J, Yan Y, Jayaraman S, Rajagopal P, Natarajan PM, Umapathy VR, Gopathy S, Roy JR, Sadagopan CS, Thalamati D, Palanisamy CP, Mironescu M. A review on advancements in the application of starch-based nanomaterials in biomedicine: Precision drug delivery and cancer therapy. International Journal of Biological Macromolecules. 2024; 130746.
[66] Pei JJ, Yan Y, Palanisamy CP, Jayaraman S, Natarajan PM, Umapathy VR, Gopathy S, Roy JR, Sadagopan JC, Thalamati D, Mironescu M. Materials-based drug delivery approaches: Recent advances and future perspectives. Green Processing and Synthesis. 2024; 13: 20230094.
[67] Pei JJ, Deng W, Liu Y, Guo Y, Chen J, Abdu H, Khan MR, Palanisamy CP, El-Aty AM. A Comprehensive Review of Cornus officinalis: Health Benefits, Phytochemistry, and Pharmacological Effects for Functional Drug and Food Development. Frontiers in Nutrition. 2023; 10: 1309963.
[68] Alugoju P, Palanisamy CP, Anthikapalli NVA, Jayaraman S, Prasanskulab A, Chuchawankul S, Dyavaiah M, Tencomnao T. Exploring the anti-aging potential of natural products and plant extracts in budding yeast Saccharomyces cerevisiae: A review. F1000Research. 2023; 12: 1265.
[69] Lavanya M, Krishnamoorthy R, Alshuniaber MA, Manoharadas S, Palanisamy CP, Veeraraghavan VP, Jayaraman S, Rajagopal P, Padmini R. Formulation, characterization and evaluation of gelatin-syringic acid/zinc oxide nanocomposite for its effective anticancer, antioxidant and anti-inflammatory activities. Journal of King Saud University-Science. 2023; 35: 102909.
[70] Palanisamy CP, Poompradub S, Sansanaphongpricha K, Jayaraman S, Subramani K, Sonsudin F. Biosynthesis of silver nanoparticles (AgNPs) using ethanolic extract of Nigella sativa (L.) seeds promotes wound healing via PDGF and VEGF signalling pathways activation. Biocatalysis and Agricultural Biotechnology. 2023; 54: 102970.
[71] Prasad M, Jayaraman S, Natarajan SR, Veeraraghavan VP, Krishnamoorthy R, Gatasheh MK, Palanisamy CP, Elrobh M. Piperine modulates IR/Akt/GLUT4 pathways to mitigate insulin resistance: Evidence from animal and computational studies. International Journal of Biological Macromolecules. 2023; 253: 127242.